IMAGE ANALYSIS OF SURF ZONE HYDRODYNAMICS

J.M.Redondo[b], A.Rodriguez[a], E. Bahia[a], A.Falqués[b]
V. Gracia[a], A.Sánchez-Arcilla[a] and M.J.F. Stive[a]

ABSTRACT: A serie of relatively novel techniques is presented to study surf-zone hydrodynamics by means of digital processing of video image recordings of the sea surface near the coast. Image analysis may be used to estimate spatial and temporal characteristics of wave fields, surface circulation, mixing and morphodynamics in the surf zone. Preliminary field measurements were conducted in May 1993 along the Ebro Delta (Spanish Mediterranean Coast), to test the methodology. Spectral analysis on the images was applied used to estimate energetic wave frequency bands as well as dispersion relations of shear instabilities. These results are compared with numerical model predictions. Results from a recent campaign at the same site in December 1993 were used to validate the analysis. Results from three days with quite different sea conditions are compared and longshore current and dispersion measurements from the tracking of dye blobs are presented.

INTRODUCTION

The study of near-shore processes, and especially the interaction between wave fields, longshore currents, turbulence characteristics and beach morphology, needs detailed measurements of the simplest possible events to understand the complexity of coastal dynamics. A step by step approach starting from a well behaved (linear) coastal area was selected.

The generation of longshore currents by wave fields has been measured and discussed in detail by e.g. Thornton (1970). Since then, many authors have shown the complexity of the wave-current-turbulence interactions which has helped to gain insight into the time and space variability of longshore currents due to e.g. edge waves and shear instabilities.

The study of coastal hydrodynamics and morphodynamics by means of aerial images has also been treted by several researchers. Sonu (1969) utilized a 35mm motor-driven photocamera to study nearshore current patterns and mixing. Sasaki and Horikawa (1972/76) improved the resolution and accuracy

---

Universidad Politécnica de Cataluña, U.P.C. Campus Nord, 08034 Barcelona, Spain, *a*: Lab. Ing. Marítima, and *b*: Dept. Física Aplicada.

for mapping the quantitative flow field in the surf zone applying the idea of Stereo-Bacs (with two baloons and 70mm motor-driven cameras). Maresca and Seibel (1976) have used land based phogrametry to measure breaking waves and longshore currents; buoys and fluorecein dyes were the tracers used. Recent work by Kuriyama and Ozaki (1993) has compared numerical model results with extensive field measurements using a 400 m long offshore pier perpendicular to a sandy beach in Hazaki, Japan. In this work the longshore current was measured by tracking tracers on the sea surface.

Since the 80's, video and digital procesing techniques have allowed flow visualization in accurate and efficient ways, for a complete description of these techniques see Hesselink (1988). The Army corps of Engs. during Duck, N.C. experiments, replaced photographic material by video, and began to explore the potential of this technique (Holman and Sallenger, 1986). The expected capabities of video recording and digital processing for the study of coastal processes include horizontal velocity fields, dye mixing, angle and period of incident waves, wave runup, surf zone width, sand bar morphology, shoreline response, etc.

Holman and Lippmann (1987/89/93) have employed extensively video techniques in the quantification of sand bar morphology. Breaking waves characteristics such as overwash bore velocities (Hollad et al., 1991), or phase speed and angle (Lippmann and Holman, 1991) have also been measured using video techniques. These authors have also quantified the long period time scales associated with breaking waves during DELILAH experiment on North Carolina, (Lippmann and Holman, 1992). Recently, the wave runup has also been measured using video records of a beach on Maryland by Walton (1993). This list shows the extensive use of these techniques, which appear to be an useful complementary tool for remote sensing (field and laboratory measurements) of coastal dynamics.

The paper starts with a description of the site, the set up of the DELTA 93/94 field experiments, and the conditions on the different days. In section three results from the image analysis are presented and compared with other measurements. The numerical model used is then discussed and its results compared with the experimental results.

FIELD WORK AND METHODOLOGY

The site chosen for this study was the Trabucador bar in the Ebro delta which has a long history of data gathering and simple linear geometry. In figure 1 a map of the area is shown together with other zones considered for the study. Two sets of measurements will be discussed in the paper, corresponding to May and December 1993. The bathymetry was measured both before and after the field campaign. A bottom elevation plot at the start of measurements on the 26th of May is shown in figure 2. On this day, the profile showed both a primary and a secondary bar. The profiles measured in December showed only a single bar, with no trace of the inner bar. This difference is due to the varying weather and sea conditions described below.

The DELTA 93/94 measurements include simultaneous time series of waves, velocities and sediment concentrations from the surf zone of this

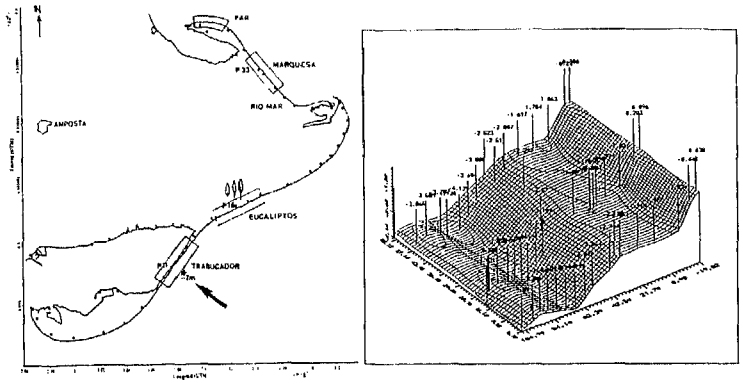

Figures 1 and 2: Map of the Ebro Delta showing the Trabucador studied area (P11), and the P11 bathymetry for 26/May/93, respectively.

microtidal barred beach, during calm and storm conditions. The main characteristics of the incident wave field were measured by means of a video camera (VTR), a directional wave rider (DWR) placed just in front of the Trabucador site, (1500 m offshore at 7 m water depth) and a X-band radar.

In the December measurements, in addition to the DWR, a conductivity type wave gauge (WG) was placed on a movable "sledge" and used to measure surf zone wave transformation. The vertical structure of the velocity field was measured by means of six electromagnetic current meters ($EMCM$) deployed in the vertical pole of the sledge. Suspended sediment concentrations were measured with three optical back-scatter sensors (OBS) and the time averaged suspended sediment transport was measured by means of two portable sediment traps (PST). These sediment transport measurements will not be discussed in here.

During the experiments video images were recorded in a S-VHS system. The BW video camera was placed in a waterproof housing at 20 m above the sea surface by means of a crane. Several fiducial points were marked with white flags both at the coastline and 60 m offshore. An elevation view, with the shore details, the equipment and the camera position is shown in figure 3. The height and orientation of the camera could be changed by means of the crane controls. Two types of video images were collected, viz. frontal and lateral views of the shoreline. The frontal imaged area ranges from the beach to the horizon in cross-shore directon (with an effectively resolvable area from the shoreline to the outer bar -200m-). In the longshore direction the images cover 150 m along the shoreline and 300 m along the inner bar (50 m from the shoreline). The most detailed measurements were restricted to the points inside the fiducial points, where the camera distortion was lower.

Quantitative information from the video images is acomplished using the *DigImage* video processing system, and an arithmetic frame grabber ($DT2861$)

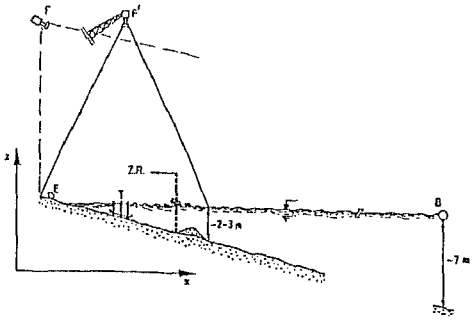

Figure 3.: A sketch of the area and equipment: E: measurement station, T: sledge with EMCM, OBS, PST and WG, B: DWR, F: video camera.

on an IBM compatible computer, which allows a resolution of 512 by 512 pixels and 256 grey levels. Images can be digitally enhanced to stretch the contrast and filter "noise" before analysis. The video may be controlled by the computer, allowing, remote control of the processing.

The images were corrected for optical deformations due to camera angle and lens distortion. World coordinates are asigned to known points marked in the video image and pixel values may be easily converted to real calibrated coordinates. The resolution in frontal view image pixels is less than 0.4 m in the cross-shore direction, and 0.1-0.4 m in the longshore direction up to the outer bar. The video recordings show clearly areas of breaking-induced turbulence and foam, which correspond to the swash zone and to first and second breaklines. See figure 4 for a false colour sequence of time averaged (equivalent to a long exposure) and instantaneous images of the area. The first bar and the swash are seen as dark bands, and contour lines are also shown.

The analized video series correspond to the three days indicated below, displaying fairly different sea conditions:

i) a post storm situation with double peaked waves coming from NE during May 26 1993. The spectrum corresponding to the time of video measurements is shown in figure 5a. The observed peaks of the spectrum were $T_{p1} = 13$ s and $T_{p2} = 3$ s. The evolution of wave heights during the day is shown in figure 6a. The storm which developed during the previous day reached a maximum in wave height in the early hours of the morning $H_{1/3} = 1.10$m. At the time of the video measurements $H_{1/3}$ was 0.5 m.

ii) a calm situation with waves coming from SE during December 15 1993. The spectra of low energy incident waves shows two close peaks corresponding to $T_{p1} = 8.3$ s and $T_{p2} = 6.6$ s ($H_{1/3} = 0.25$m according to *DWR* data). See figure 5b for the wave spectrum and figure 6b for the evolution of the $H_{1/3}$. An arrow indicates the time of detailed

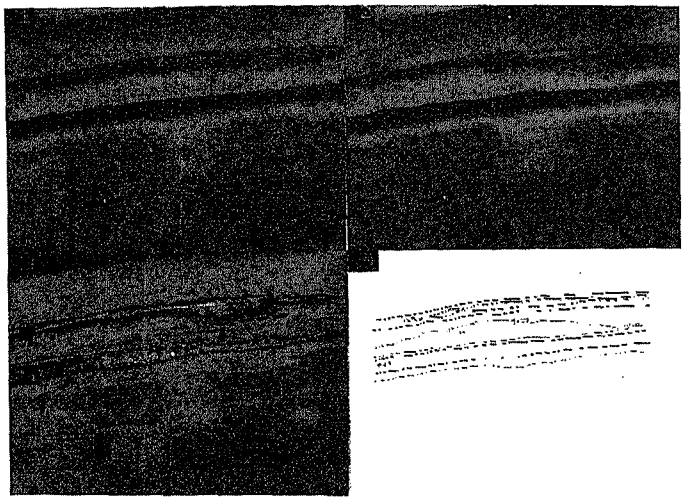

Figure 4: (1-2) Averaged images of the surf-zone, (3) single frame and (4) isolines of intensity.

measurements.

iii) a moderate situation storm with waves coming from SE during December 16 1993. The spectra shows a dominant peak at 7.1 s with lower energy signatures corresponding to a low frequency oscillation (T=18.3 s) and to a higher wave frequency with period of T=5.1 s, see figure 5c. The wave height evolution during the day is shown in figure 6c where the passage of the storm produce an increase of $H_{1/3}$ between 0.50 - 0.80 m. The video and *WG* data where obtained around 16 h GMT (shown with an arrow). The $H_{1/3}$ during the experiment was 0.6 m.

Spectral analysis of VTR/WG/DWR time series

Three types of time series were used in the spectral analysis: intensities from video images (*VTR*), water level oscilations from the *WG* and the *DWR*. The sampling intervals were respectively 0.20-0.60-1.64 s, 0.25 and 0.78 s. The length of the time series corresponding to video images were 100-300-840, and 1200 s for both *WG* and *DWR*.

The time series were detrended using a simple linear regression tapered with a Welch window prior to applying FFT. The raw spectra have been calculated over series with a minimum of 512 points grouped in subseries of 128 records (50 % overlapped). After that a high pass filter with a folding frequency of 0.000001 Hz has been used to eliminate the undesired frequencies. The associated spectral variance was 14 %.

The intermediate frequency wind wave components and the infragravity

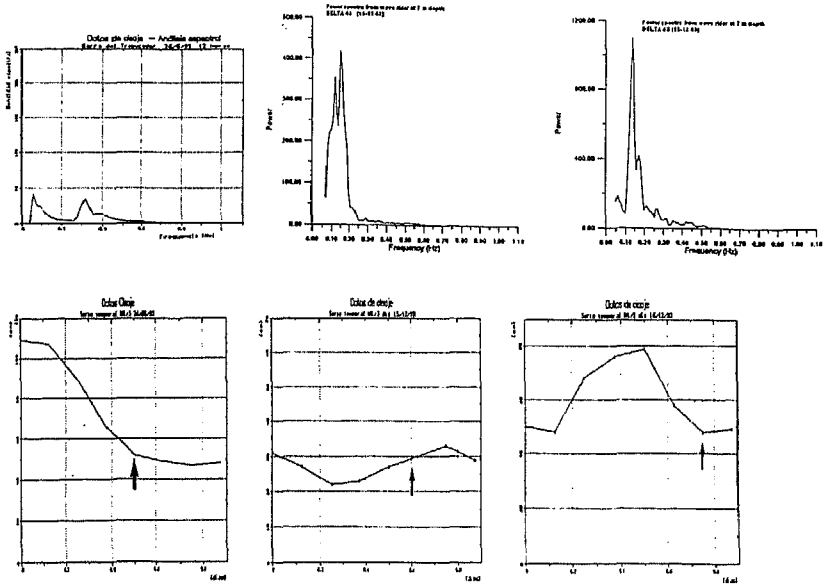

Figures 5 and 6:Measured wave spectra and $H_{1/3}$ evolution respectively for the three selected days: 26 May, 15 and 16 December 1993.

and shear instabilities were investigated. Due to the short time series used in the video data (up to 15 min), the low frequency ranges had to be handled with extreme caution.

FIELD RESULTS

The use of time series of horizontal and vertical pixel intensities allowed to measure wave frequencies, as well as the longshore component of the velocity thanks to the traces of advected surf (foam). In figure 7(1-4) an example of the time evolution (vertical) of the color coded reflected light intensities of a line is shown at four locations offshore.

Fast Fourier transform (FFT) methods applied to the digitized video images and to their correlations were used to detect the dominant wavenumbers and wave directions. Time averaged spatial images and time series of a transect (see figure 8) are seen to be convenient techniques for the characterization of wave fields. The relationship between light intensity, which has been the main parameter studied, and the surface elevation needs further study, but it is clear that for the non breaking waves, the angle between the wave surface, (bisecting the sun direction), and the video camera, will produce a maximum reflected intensity. This is also true for cloud covered skies. In addition, wave breaking,

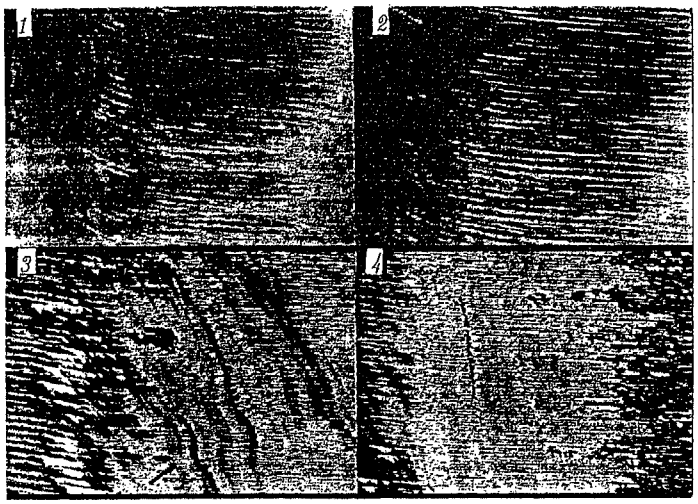

Figure 7: Time series of colour coded reflected light intensity showing the drift of surf. Ligth areas indicates wave breaking, (1) area behind the bar, (2) inside near the bar, (3) between the bar and the swash, (4) swash area. See in figure (3) the oscillations of the longshore current.

can be clearly seen and whitecaps may be easily traced.

Power spectra across-shore

Analysis of breaking and non breaking time series of 100, 300 and 840 s length and their intensity power spectra are presented as a function of cross-shore distance. These image spectra are then compared with WG and DWR spectra. In figure 9 the intensity spectra of four points near the WG structure are presented, together with the spectrum obtained from the WG data. The agreement, as seen in this figure, is very good.

i) 26/May/93: Four long time series of 300 s are presented in figure 10(a), and their respective spectra in figure 10(b). The intensity series are presented with an offset of 20 in the range 0-256 given by the digitizer resolution. The spectra from the longer series (including several 840 s series) are compared with low frequency shear waves obtained from the numerical model described below. The sites chosen were the outer bar, the inner bar, the trough and the swash zone. The dominant frequencies were: a low frequency oscillation with period of 77 s and a wave induced peak of period 6 s, which appeared in all positions. The DWR spectra for the incident wave field showed dominant waves of periods 13 s and 2 s. The incident wave groups appeared to merge, giving a dominant period of 6 s. At the swash zone the intensity variations are much larger, as seen in figure 11, and other significant periods are found at 19 s, 11 s and 7.7 s.

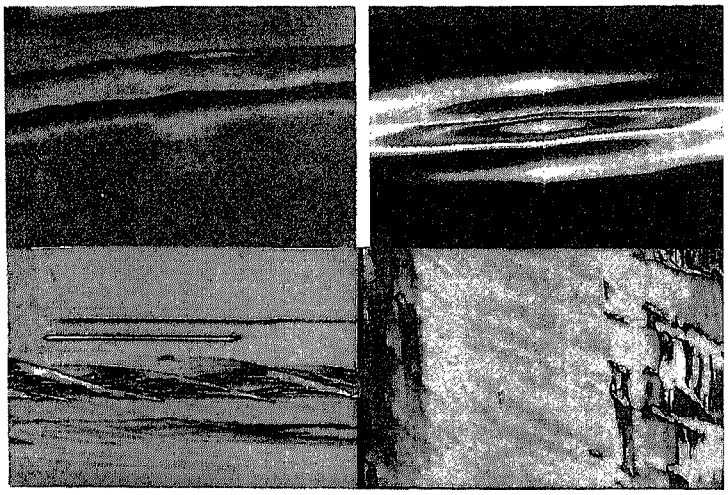

Figure 8: (Top/left) Colour coded intensity of a time averaged image showing the average surf zone width, (Top/right) Auto correlation function of the previous image showing the prefered directions, (Bottom/left) Time series of the central vertical line of the frave showed above showing period and direction of the incident waves, (Bottom/rigth) Time series of the central horizontal line. showing surface velocities across the surf zone.

ii) 15/December/93: The evolution of wave frequencies with cross-shore distance was investigated using 100s video intensity time series in order to resolve wave generated frequencies. The seven selected cross-shore positions are described in figure 11(a), and the agreement with the DWR was also good, measuring a period of 6.4 s from the video images, and a period of 6.6 from the DWR showed in figure 11(b). Other periods detected at the DWR were 8.3 s and 10.5 s. A transition from the 6.6 s period, (DWR dominant incident waves) to the recorded periods at the WG of 7.9 s and 2.8 s could be followed with the aid of the video images.

As mentioned above, the dominant waves at a position offshore, in the vicinity of the DWR have a period of 6.4 s. At the outer bar, where there is very little breaking, during calm conditions, the 6.4 s waves are mantained, but some period doubling occurs and a 12.8 s peak appears. In addition, waves of period 4.2 s are also generated near the outer bar. During these experiments, the position of the WG was just outside the surf zone and the video images near it show dominant periods of 6.6 s and 2.9 s just before to the surf zone. The observed periods are also 6.6 s and 2.9 s, with a new developing period of 4 s. There is some breaking at the surf zone which generates some new spectral peaks. Inside the surf zone, the dominant peak corresponds to 8.5 s. and there are smaller peaks corresponding to wave periods of 5.1 s and 3.6 s.

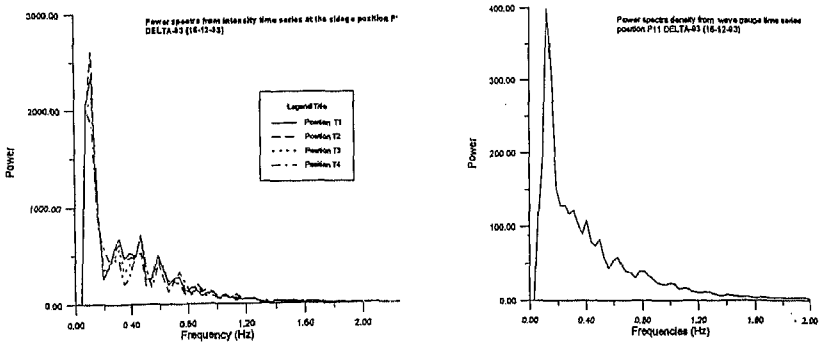

Figure 9: Comparison of spectra from WG data and video intesities at the same position.

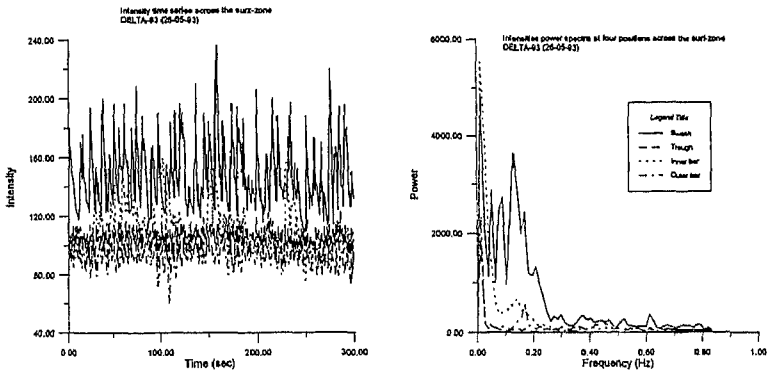

Figure 10: (a) Intensity time series,(b) Intensity spectra of four cross-shore positions.

It is interesting to note waves of period 8.5 s, which are close to some of the incident wave periods at the *DWR*. At the swash zone the dominant period is of 12.8 s, with a secondary one at 2.8 s, and at the shore line, the periods are 5.1 s and again 12.8 s.

The interpretation of this spectral cross-shore evolution is as follows: due to the low energy of the incident wave field, the dominant wave field interacts with the outer bar producing a reinforcement of every other wave. The intermediate 7.9 - 8.5 s waves appear only outside the surf zone and inside the trough, where the breaking distorts the periodicity, as may be seen in a video

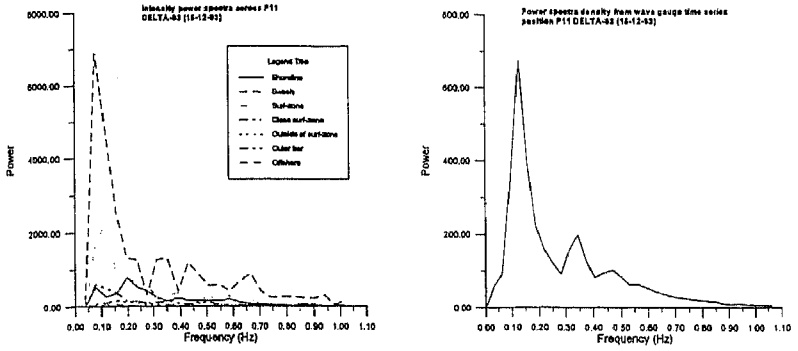

Figure 11: (a) Intensity spectra of seven cross-shore positions, (b) spectra from the WG.

image of a time evolution of a line inside the surf zone (figure 12). Finally the long (slow) waves ($T = 12.8$ s) break against the shore with some superimposed faster wave components.

Figure 12: Intesity time serie at a horisontal line showing wave distortion across the surf sone.

iii) 16/December/93: The evolution of wave frequencies with cross-shore distance was investigated using 100s video intensity time series. The sites chosen are described in figure 13, where the spectra are also shown.

The agreement with the DWR was also good, and a transition from the

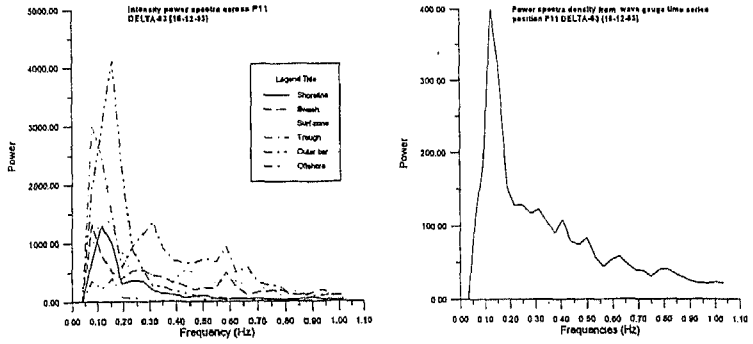

Figure 13: (a) Intensity spectra of six cross-shore positions,(b) spectra from the WG.

6.4 s period waves to the 8.0 s waves detected at the *WG* could be followed as waves approached the coastline. The offshore video spectra, (closer than the *DWR*) shows dominant periods of 1.8 s 6.4 s and 12.8 s , as in the previous day. The *DWR* during the time of video measurements showed periods of 5.8 s and 7.1 s, which are close enough to the 6.4 s. This period is seen at several locations, but not at the trough, where the *WG* was placed. The *WG* measurements show wave periods of 3.2 s and 8 s, just offshore the position where the *WG* video measurements showed periods of 1.7 s , 3.2 s and 12.8 s. Closer to the surf zone, periods of 2.3 s, 3.2 s and 8.5 s are detected. At the swash zone, the periods are 3.6 and 12.8, again a multiple of the offshore one, and at the shoreline 1.9 s , 4.2 s and 8.5 s periods are detected.

The main aim of the spectral analysis presented here for the December campaign is to show that much more spatial information may be quantitatively obtained at wave spatial and temporal ranges. The use of light intensity data in order to describe wave frequencies and their structure was used by Lippmann and Holman mostly for breaking waves, but due to the good resolution of the images, changes in the sea surface angle could also be detected with the present data. In order to justify the use of the video time series, a detailed comparison was made with the *WG* data and the video intensity series for the december campaign.

The measurements with longer video time series have not been as successful in revealing the infragravity wave range and the longer periodicities, mostly due to the lack of sufficiently long and steady measurements.

Dye dispersion measurements

Measurements of dye dispersion at different distances from the shore (inside the surf zone) have been used to obtain estimates for longshore current and turbulence characteristics, such as the mean Lagrangian trajectories, mean and r.m.s. velocity integral lengthscales, shape and anisotropy of blobs, etc.

The tracers were selected after field intercomparisons of different substances (fluoresceine, rhodamine, MnO_4K_2, SO_4Ca and milk). The best tracer varies depending on weather conditions because of the difference of constrast between dye and marine water, but milk and fluoresceine were the best ones because of their good contrast and persistance. Figure 14 shows a time averaged image during 30 seconds of dye trajectory (20 gr of fluoresceine).

Figure 14: Average picture obtained integrating point video intensities during 30s as one of the dye blobs is released. The trajectory may be identified near the center of the image.

From dye dispersion measurements and from the evolution of intensity isolines, fractal measures of selfsimilarity ranges and of dominant scales are also obtained. The spatial and time evolving characteristics of the surface velocity fields, are used to complement the vertical velocity profiles obtained by means of electromagnetic current meters.

NUMERICAL MODEL RESULTS

Numerical longshore currents models have been used to predict the most relevant modes taking into account the measured boundary conditions. The dispersion relations and pattern of edge waves for the actual bathymetry and longshore current have been computed using the numerical method described in Falques and Iranzo (1992). The steady longshore current profile has been computed with an incoming wave height of 0.46 m, and an incidence angle of 23.4°. Under the assumption of alongshore uniformity, the occurrence of shear instabilities of the longshore current has also been investigated by means of a numerical simulation. For this purpose, the basic current profile (Figure 15 c) and the lateral momentum diffusion distribution (Figure 15 b) have been obtained from the incident wave field applying a propagation and circulation model (Rivero and S.Arcilla, 1991) and the measured bathymetry (Figure 15 a).

The longshore current profile has two peaks: the strongest one near the shoreline with $V_m \simeq 0.46 m/s$ and maximum backshear $f_s \simeq 0.08 s^{-1}$ and the weaker one over the inner longshore bar with $V_m \simeq 0.13 m/s$ and maximum backshear $f_s \simeq 0.0007 s^{-1}$. Similarly, the eddy viscosity coefficient distribution has also two peaks of about $0.04 m^2 s^{-1}$. A constant drag coefficient of $c_d = 0.0015$ has been taken for bottom friction.

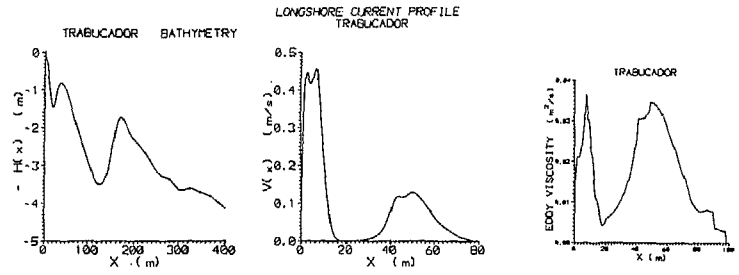

Figure 15: (a) Bathymetry, (b) eddy viscosity and (c) computed longshore velocity profiles at P11 considered in the shear instabilities simulation.

The shear instability analysis started from the shallow water equations

$$\frac{\partial v_i}{\partial t} + v_j v_{i,j} + g\eta_{,i} = -\frac{c_d}{h}|\vec{v}|v_i + \frac{1}{h}S_{ij,j} + \frac{1}{h}[\epsilon h(v_{i,j} + v_{j,i})]_{,j} \qquad i = 1,2 \quad (1)$$

$$\frac{\partial \eta}{\partial t} + [hv_j]_{,j} = 0 \qquad (2)$$

followinf the approach of Falqués and Iranzo, 1994 (hereinafter FI94). A linear stability analysis has been performed by assuming perturbations with the form

$$e^{(\omega_r + i\omega_i)t} e^{iky} v'(\vec{x}),$$

where $k = 2\pi/\lambda$. The same spectral method of FI94 based on rational Chebyshev expansions has been used here. However, the present calculation uses bathymetry, current and eddy viscosity interpolated from the experimental data. The considered eddy viscosity coefficient, $\epsilon(x)$, has therefore a cross-shore variation.

Two linear unstable shear modes have been found. As it can be seen in Figures 16(a-b) ,the dominant one has a fastest growing wavelength about $\lambda = 31m$, a period $T = 104s$ and a growth rate $\omega_i = 0.006s^{-1}$. The other one has $\lambda = 70m, T = 1000s$ and $\omega_i = 0.0018s^{-1}$. Figure 16(c) shows the cross-shore structure of both modes.

Since the dominant mode is located near the shoreline it appears to be associated with the strongest current peak. On the other hand, the other mode is distributed in a wider region centered at the inner bar. Therefore, it is likely associated to the lowest current peak. Assuming this correspondence, both solutions agree quite well with the rough predictions for plane beach and inviscid flow in FI94. For instance, the phase speed to peak longshore current ratio, is $c_1/V_{m1} = 0.65$ for the first mode and $c_2/V_{m2} = 0.54$ for the second one. Further,

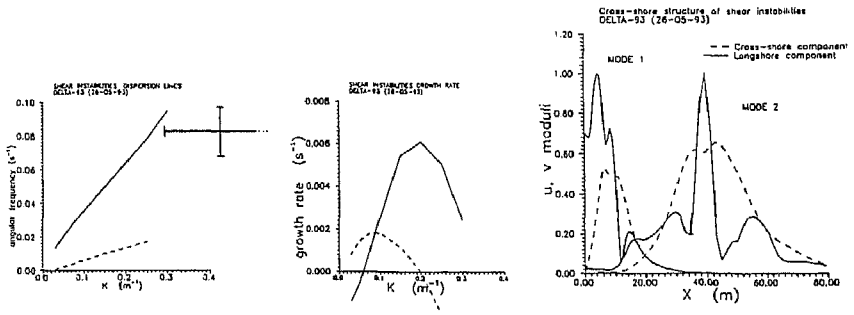

Figure 16: Linear unstable shear modes.

the wavelength to current width ratio is about 1.7 for the first mode and 2.3 for the second one. According to the estimates for inviscid flow in FI94, growth rates should be around $\omega_i \sim 0.1 f_s$. For the second mode this would give 0.008 s^{-1} whereas the present calculation gives 0.006 s^{-1}, which shows a small decrease due to dissipation. However, for the second mode the inviscid estimate gives 0.0007 s^{-1} and the present calculation (which takes dissipation into account) gives 0.0018 s^{-1}. Dissipation seems to de-stabilize the flow in this case. Which is in line with some recent calculations for a more general situation where it was found that some eddy viscosity distributions may in some cases destabilize the basic flow.

In order to estimate dispersion relations from the field measurements, two methods were used: the first one was to consider the low frequency amplitude spectrum peaks as indications of slow sea surface undulations. The estimates range between 70 s and 84 s. A clearer indication of the shear instability may be the recorded oscillations in the longshore current, in which dye (milk and fluorescein) blobs sometimes showed large mean velocity oscillations as noted in figure 17 (a). In this figure the evolution of dye spots may be seen for two days with opposing longshore currents.

Quantitative measurements for the period of oscilation of the longshore current can be seen in figure 7(3). The oscillations of the longshore current on the 26th of May were of the order of 100 s. The lengthscales corresponding to the largest waves obtained by means of spatial fourier transforms in the trough lie between 10 and 20 m, which give an estimate of T and λ. These data are also plotted for comparison in figure 16 (c), together with the dispersion relation for the 1st and 2nd shear instability modes.

CONCLUSIONS

Digitized video images of field events seems a promising technique for

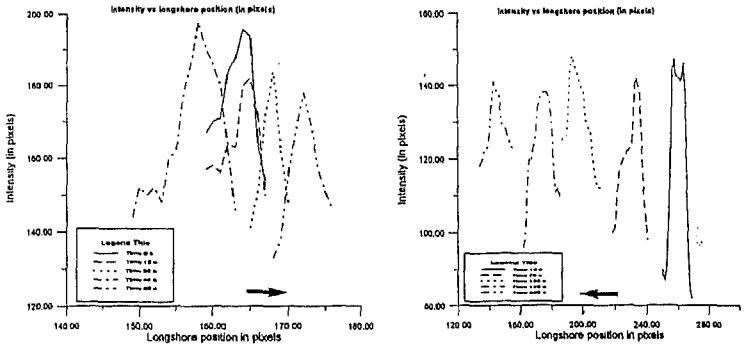

Figure 17: Blob evolution from video images, (a) 26/May/93 and (b) 15/December/93.

extended quantitative measurements of sea surface instabilities. The agreement between Video spectra and DWR and WG is qualitatively good and allows to describe in more detail the global characteristics of the surf zone.

The evolution of wave characteristics as they interact with the surf zone may be followed in detail. The outer and the inner bars act as a filter to some frequencies that reapear near the shoreline or at the trough, the variation of frequencies being clearer for the more energetic sea conditions.

The non-linear effect of the surf zone is apparent in enhanced images, such as figure 14. There is a process of wave dislocations, between the surf and swash zones that needs further study. This is also reflected in the changes in dominant wave period as the waves approach the coastline, from measurement with image analysis. The dynamic response of the surf zone to different incoming wave fields may be, thus, investigated in detail.

The numerical model shows some agreement in time scales for the dispersion relationship, but the spatial scales are somewhat lower than predicted. Considering that the model is linear and several approximations (e.g. constant bottom drag) have been used, there seems to be ground for improvement. In future models other important effects, like variable friction should be taken into account.

The measured longshore current at the position where the dye blobs were released is of 0.5 ms^{-1}, which agrees well with the predicted maximum longshore currents, see figure 17. The detailed longshore velocity distribution needs further comparison with field data. In the December campaign, several series of simultaneous blobs were released at different cross-shore locations and further work will include comparisons between these measurements and the numerical models.

AKNOWLEDGEMENTS

This work was undertaken as part of the Surf Zone Research project of LIM-UPC. It was funded jointly by the Programa de Clima Marítimo PCM-MOPTMA and the Ministerio de E. y C. (DGICYT) of Spain, with some support from the MAST-II Euromarge contract of the EU. We want to thank the research staff of LIM-UPC, particularly to J. Gomez, F. Rivero, J. Sospedra and all those who endured the field work. Thanks are also due to G. Voulgaris and M.A. Tenorio from Southampton University for their OBS and radar, and research staff of DFA-UPC, particularly to V. Iranzo and D. Crespo.

REFERENCES

Falqués,A. and Iranzo,V., 1992. "Edge waves on a longshore shear flow", *Physics Fluids A 4 (10),* 2169-2190.

Falqués,A. and Iranzo,V., 1994. "Numerical Simulation of Vorticity Waves in the nearshore, *J.Geophys Res.* 99, (C1), 825-841 (1994).

Hesselink,L., 1988. "Digital Image processing in flow visualization" *Ann. Rev. Fluid Mech.*, 20, 421-485.

Holland,K.; Holman,R. and Sallenger,A., 1991. "Estimation of overwash bore velocities using video techniques" *Coastal sediments* ASCE, 489-497.

Holman,R. and Sallenger,A., 1986. "High-energy nearshore processes" *EOS* Trans. Americ. Geoph. Union, December 9, 1369-1371.

Holman,R. and Lippmann,T., 1987. "Remote sensing of nearshore bar systems - making morphology visible" *Coastal sediments* ASCE, 929-944.

Kuriyama,Y. and Ozaki,Y., 1993. "Longshore current distribution on a bar-trough beach" Report of Port and Harbour Research Institute. Japan. Vol. **32. 3**, 3 - 37.

Lippmann,T. and Holman,R., 1989. "Quantification of sand bar morphology: a video technique based on a wave dissipation", *J.Geophys.Res.* Vol 94, No C1, 995-1011.

Lippmann,T. and Holman,R., 1991. "Phase speed and angle of breaking waves measured with video techniques" *Coastal sediments* ASCE, 542-556.

Lippmann,T. and Holman,R., 1992. "Wave group modulations in cross-shore breaking patterns", Proc. I.C.C.E., ASCE, 918-931.

Lippmann,T., Holman,R. and Hathaway, K., 1993. "Episodic, nonstationary behavior of a double bar system at Duck, N.C., USA, 1986-1991" Jour. of Coastal Reseach, **SI,15**, 49-75.

Maresca,J. and Seibel,E., 1976. "Terrestrial photogrametric measurements of breaking waves and longshore currents in the nearshore zone", Proc. I.C.C.E., ASCE, 681-700.

Sonu,C., 1969. "Tethered balloon for study of coastal dynamics", Amer. Soc. Photogram., Tech. Rep., 66, 91-103.

Thornton,E.B., 1970.- "Variation of longshore current across the surf zone" Proc. I.C.C.E., ASCE, . **12.** , 291-308.

Sasaki,T., Horikawa,K. and Hotta,S., 1976. "Nearshore current on a gently sloping beach" Proc. I.C.C.E., ASCE, . **36.**, 626-644.

Rivero,F. and Sánchez Arcilla,A., 1991. "Quasi-3D nearshore current modelling", *Computer Modelling in Ocean Engineering 91*, Balkema, 171-178.

Walton,T., 1993. "Ocean City, Maryland, wave runup study" Jour. of Coastal Reseach, **9,1**, 1-10.